JCTC Journal of Chemical Theory and Computation

ARTICLE

pubs.acs.org/JCTC

Direct Calculations of Mid- and Near-IR Absorption and Circular Dichroism Spectra of Chiral Molecules Using QM/MM Molecular Dynamics Simulation Method

Jun-Ho Choi[†] and Minhaeng Cho[*,†,‡]

[†]Department of Chemistry, Korea University, Seoul 136-701, Korea

[‡]Multidimensional Spectroscopy Laboratory, Korea Basic Science Institute, Seoul 1360-713, Korea

ABSTRACT: The infrared (IR) and vibrational circular dichroism (VCD) spectra of (1*S*)-(−)-β-pinene in the mid- and near- IR frequency regions are numerically simulated by using a time-correlation function theory and mixed quantum/classical simulation method. Anharmonic vibrational dynamics and fluctuating atomic partial charges of the chiral pinene were obtained by carrying out quantum mechanical/molecular mechanical (QM/MM) molecular dynamics (MD) simulations. Thus obtained time-correlation functions of electric and magnetic dipole moments are used to calculate the IR absorption and VCD spectra, and they are directly compared with experimental results. Not only the fundamental transition bands but also first overtone and combination bands in the near-IR frequency region are successfully simulated. It is shown that the polarizable nature of the solute is particularly important in quantitatively reproducing the near-IR spectra, whereas such polarization effects on dipole and rotational strengths of lower-frequency and large-amplitude vibrations are less critical. We anticipate that the present QM/MM MD method in combination with mixed quantum/classical time-correlation function theory to calculate both mid- and near-IR absorption and VCD spectra will be of critical use in interpreting vibrational optical activity properties of even conformationally flexible chiral molecules, such as proteins.

1. INTRODUCTION

Near-infrared (NIR) spectroscopy uses near-infrared region of the electromagnetic field in the wavelength range from 800 nm to 2.5 μm.[1] Within this wavelength range, molecular overtone and combination vibrations can be resonantly excited.[2,3] Such transitions are, however, quantum mechanically forbidden within the harmonic approximations to molecular vibrations so that their oscillator strengths are often 1 or 2 orders of magnitude smaller than those of fundamental transitions, which makes it difficult to use as a sensitive technique. However, a notable advantage of NIR spectroscopy is its ability to penetrate farther into a sample than mid-infrared or visible radiation. Thereby, it has been used in the analyses of blood hemoglobin levels, pharmaceuticals, combustion products, and even atmospheres of cool stars.[4−7]

Typically, the molecular overtone and combination absorption bands in such NIR regions are quite broad and complicated with multiple peaks. Therefore, assigning specific spectral features to particular quantum transitions and chemical components has been extremely challenging.[8,9] To enhance the frequency resolution of the NIR transition bands and to extract detailed information on absolute configuration of chiral molecule, the NIR vibrational circular dichroism (NIR-VCD) spectroscopy has been used.[10−22] In 1976, Keiderling and Stephens for the first time measured the NIR-VCD spectrum of the C−H stretching overtone and C−H stretching/C−H bending combination bands of camphor dissolved in CCl_4 solution.[16] Recently, Nafie and Abbate groups have reported the NIR-VCD spectra of chiral organic molecules including terpenes.[11,19,21−23] The C−H stretching first and second overtones, C═O stretching second overtone, and various combination modes of C−H stretching and bending, C−C stretching, C═C stretching, and O−H stretching and bending have been observed in the NIR absorption and VCD spectra of which frequency range is from 4000 to 10 000 cm^{-1}.[11]

In parallel with these experimental efforts, a number of novel attempts to numerically simulate the NIR absorption and VCD spectra by using ab initio quantum chemistry calculation methods have been reported recently.[20,24−29] For example, Abbate and co-workers used the local mode approximation,[8,9,30−32] which was initially developed by Child and Henry, for C−H stretching vibrations of camphor and camphorquinone and presented the simulated NIR-VCD spectra of C−H stretching overtone ($\Delta\nu$ = 3) transition at ∼8500 cm^{-1}.[33] The C−H stretch local mode was treated as a Morse oscillator[34] so that the matrix elements of coordinate and momentum operators could be calculated by using analytical expressions for the vibrational wave functions of the Morse oscillator. The coordinate-dependent atomic polar and axial tensors that are needed to determine dipole and rotational strengths of vibrational excitations were calculated by using a density function theory method, i.e., B3LYP/6-31G**. Their calculation method for simulating C−H stretching NIR spectra was shown to be quite successful.[33] However, such approaches may not be easily extended to simulate the NIR spectra for a variety of combination bands other than C−H stretching overtones as well as those of conformationally flexible molecular systems, since the complicated electric and mechanical anharmonicity effects on transition frequencies and electric and magnetic dipole moments are increasingly difficult to take into consideration by using such quantum chemistry calculation method for an isolated chiral molecule.[10,35]

Received: September 20, 2011
Published: November 10, 2011

In addition, the solvent−solute interaction-induced polarization and line-broadening effects on the NIR absorption and VCD spectra could not be taken into account by considering isolated molecules.

In order to overcome these limitations of ab initio calculation approaches, molecular dynamics (MD) simulation method combined with an electronic structure calculation method has recently been used to simulate IR and VCD spectra of chiral molecules in solutions.[36−46] For instance, Yang and Cho numerically simulated the IR absorption spectrum of *N*-methylacetamide (NMA) in water, directly calculating the electric dipole autocorrelation function of the NMA that is treated with a semiempirical quantum mechanical (QM) method and analyzing the QM/MM MD trajectories.[41] Later, a Hartree−Fock (HF)-QM/MM MD simulation method was used to simulate both IR absorption and VCD spectra of blocked alanine (Ac-Ala-NHMe) in water by carrying out Fourier transforms of the correlation functions of electric and magnetic dipole moments.[40] Such a QM/MM MD simulation method combined with time-correlation function theory for IR absorption and VCD spectroscopy was shown to be quite useful even for molecular systems with shallow potential energy surfaces with thermally accessible multiple conformations.[40,47,48] The fundamental transition bands thus obtained were in fair agreement with experimental results.[49] Here, it should be emphasized that the present approach with QM/MM MD simulation method combined with time-correlation function theory has an advantage in taking into account fluctuating potential anharmonicity and its effects on mode couplings, vibrational frequencies, and forbidden transition moments, since the on-the-fly QM calculations of the solute correctly include all the possible anharmonic effects that cannot be correctly taken into account with fixed charge MM simulations. Thus, it is not necessary to use a theoretical model based on local mode basis nor to carry out approximate finite-difference calculations of a variety of mechanical and electric anharmonic properties. Other notable examples demonstrating the use of QM/MM MD simulation methods in the molecular spectroscopy are needed to be mentioned here. Ringer and MacKerell calculated the vibrational frequency shifts of the CN stretching mode of acetonitrile in two different solvent environments.[50] Corcelli and co-workers considered C−D stretching mode of Ala-d_1 in an aqueous solution and successfully showed that the multiple absorption peaks found in the 2000−2300 cm^{-1} region in fact result from Fermi resonances with fundamental C_α−D stretching vibration.[38]

In this paper, we shall present QM/MM MD simulation results of the (1*S*)-(−)-*β*-pinene in CCl_4 solution to simulate both mid- and near-IR absorption and VCD spectra. This is the first attempt to directly calculate such NIR spectra by using time-correlation function approaches combined with a mixed QM/MM method. The simulated NIR absorption and VCD spectra exhibiting both C−H stretching first overtone and various C−H stretching/C−H bending combination bands of (1*S*)-(−)-*β*-pinene are directly compared with experimental results reported by Guo et al. in ref 11.

2. COMPUTATIONAL METHOD

The molecular structure of (1*S*)-(−)-*β*-pinene is shown in Figure 1. This pinene was treated quantum mechanically with HF/6-31G method in the present QM/MM MD simulation studies, where 186 CCl_4 solvent molecules were treated classical

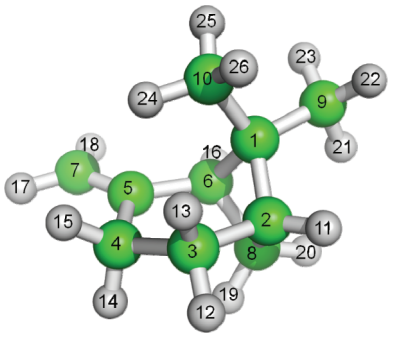

Figure 1. Molecular structure of (1*S*)-(−)-*β*-pinene. The atom types are also shown in this figure (see Table 1 for average Mulliken partial charges and standard deviations).

mechanically with CHARMM[51] force fields (version c33b2). To carry out the QM/MM MD simulation, we used the CHARMM program interfaced with GAMESS-UK[52] electronic structure package (version 7.0). A single solute molecule was placed at the center of a spherical solvent cluster with radius of 25 Å. A restraining harmonic potential was used to prevent evaporation of solvent molecules at 273 K. The solute−solvent cluster system was first minimized with the steepest descent and adopted basis Newton−Raphson methods for 100 steps each, and then the system was heated to 273 K and equilibrated for 25 ps. Simulation time step used was 0.5 fs, and totally 1 ns production run was performed. Cartesian coordinates, velocities, and atomic partial charges of the solute were saved for every 1.0 fs for subsequent calculations of electric and magnetic dipole moment trajectories. The spectral range of the simulated vibrational spectra is determined by the Nyquist critical frequency $f_c = 1/(2\Delta_t)$, where Δ_t corresponds to the data saving time step of 1 fs.

Now, using the QM/MM MD trajectory with saved atomic Mulliken partial charges of the solute, we could obtain the fluctuating electric and magnetic dipole moments, denoted as $\boldsymbol{\mu}(t)$ and $\mathbf{M}(t)$, respectively, where they are defined as

$$\begin{aligned} \boldsymbol{\mu}(t) &= \sum_i q_i(t)\mathbf{r}_i(t) \\ \mathbf{M}(t) &= \frac{1}{2c}\sum_i q_i(t)\mathbf{r}_i(t) \times \mathbf{v}_i(t) \end{aligned} \tag{1}$$

Here, $q_i(t)$, $\mathbf{r}_i(t)$, and $\mathbf{v}_i(t)$ represent the partial charge,[53] position, and velocity of the *i*th solute atom. In this work, we used the atomic Mulliken partial charges instead of Löwdin charges, because the numerically simulated VCD spectrum of the C−H stretching vibrations with the former charges is found to be in better agreement with the experimentally measured spectrum. The atomic partial charges explicitly depend on time due to solute−solvent interaction-induced charge response and conformational fluctuation of the solute molecule. Thereby, such polarizable nature of the solute molecule is naturally taken into account by the present QM/MM MD simulation method. Using thus obtained electric and magnetic dipole moment trajectories, one can readily calculate the autocorrelation function of the electric dipole moment as well as the cross-correlation function between the electric and magnetic dipole moments. Then, the IR absorption ($A(\omega)$) and VCD ($\Delta A(\omega)$) spectra can be directly calculated by carrying out the following Fourier transformations of the corresponding time-correlation

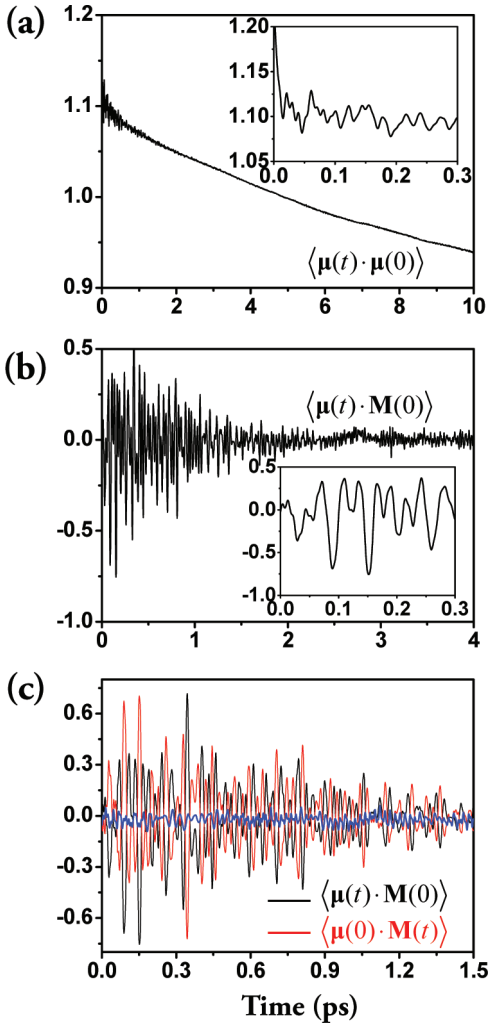

Figure 2. Time-correlation functions $\langle \boldsymbol{\mu}(t)\cdot\boldsymbol{\mu}(0)\rangle$ and $\langle \boldsymbol{\mu}(t)\cdot\mathbf{M}(0)\rangle$ are shown in (a) and (b), respectively. The dimensions of $\langle \boldsymbol{\mu}(t)\cdot\boldsymbol{\mu}(0)\rangle$ and $\langle \boldsymbol{\mu}(t)\cdot\mathbf{M}(0)\rangle$ are in D^2 and 10^{-4} $D\mu_B$, where D and μ_B are debye and bohr magneton. The first 300 fs portions of $\langle \boldsymbol{\mu}(t)\cdot\boldsymbol{\mu}(0)\rangle$ and $\langle \boldsymbol{\mu}(t)\cdot\mathbf{M}(0)\rangle$ are shown in the inset of (a) and (b). The two correlation functions, $\langle \boldsymbol{\mu}(t)\cdot\mathbf{M}(0)\rangle$ (black line) and $\langle \boldsymbol{\mu}(0)\cdot\mathbf{M}(t)\rangle$ (red line), which are to be mirror images in an ideal case, are plotted in (c). The sum of the two is the blue line in (c).

functions, i.e.,[40,54]

$$A(\omega) \propto \int_{-\infty}^{\infty} dt e^{i\omega t}\langle \boldsymbol{\mu}(t)\cdot\boldsymbol{\mu}(0)\rangle \quad (2)$$

$$\Delta A(\omega) \equiv A_L(\omega) - A_R(\omega) \propto \mathrm{Im}\int_{-\infty}^{\infty} dt e^{i\omega t}\langle \boldsymbol{\mu}(t)\cdot\mathbf{M}(0)\rangle \quad (3)$$

where $A_L(\omega)$ and $A_R(\omega)$ are the absorption spectrum measured by using a left and right circularly polarized radiation. respectively. A detailed theoretical description on the time-correlation function formalism of the VCD spectrum can be found in ref 40.

3. SIMULATED IR ABSORPTION AND VCD SPECTRA

3.1. Time-Correlation Functions. The two time-correlation functions, $\langle \boldsymbol{\mu}(t)\cdot\boldsymbol{\mu}(0)\rangle$ and $\langle \boldsymbol{\mu}(t)\cdot\mathbf{M}(0)\rangle$, calculated with eq 1 are shown in Figure 2. It turns out that, even though the overall

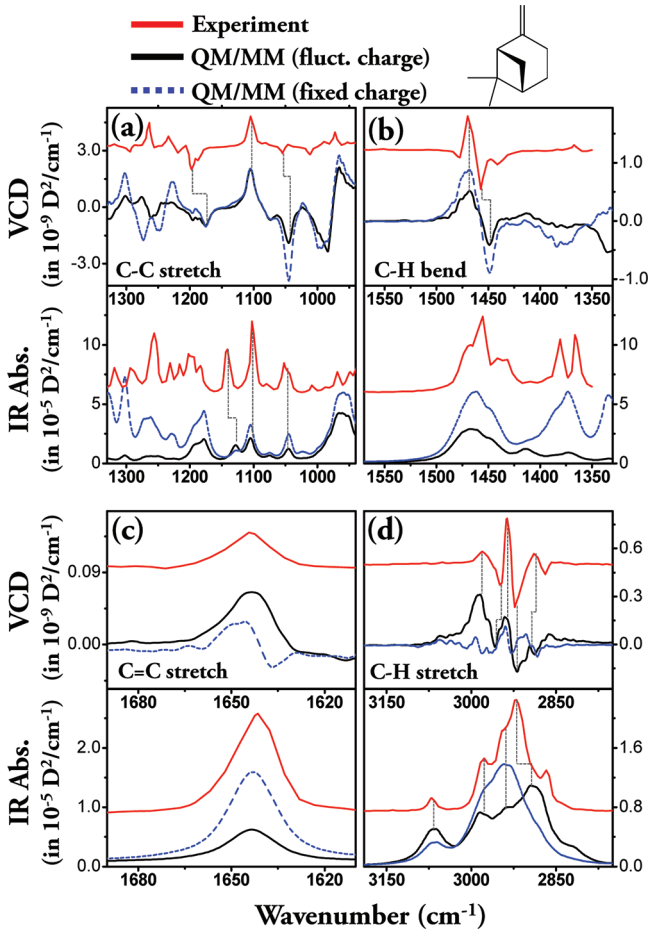

Figure 3. Numerically simulated IR and VCD spectra of (1*S*)-(−)-*β*-pinene. Those of C−C stretch (a), C−H bend (b), C═C stretch (c), and C−H stretch (d) modes are shown in this figure. The red lines represent experimentally measured IR absorption and VCD spectra reported in ref 11. The black lines represent the simulated spectra obtained by using the QM/MM MD simulation trajectory and eq 1 so that the fluctuating charges were properly taken into account. The blue lines however correspond to the simulated spectra with fixed atomic partial charges (see Table 1). Here, the frequency correction factors for the C−C stretch, C−H bend, C═C stretch, and C−H stretch modes are 0.8701, 0.8739, 0.8779, and 0.8953, respectively. Also the corresponding lifetimes are assumed to be 1 ps and 800, 600, and 500 fs. Note that the IR absorption and VCD intensities are given in 10^{-5} and 10^{-9} D^2/cm^{-1}, respectively.

absorption and VCD line shapes are clearly discernible, the direct Fourier transforms of these correlation functions appear to be quite noisy due to the limited length of QM/MM MD trajectory. Furthermore, the intrinsic lifetime-broadening contribution to the simulated spectra could not be taken into account, since the QM/MM MD simulations were performed at a thermal equilibrium condition. Therefore, we approximately describe the lifetime effect by multiplying an exponential function of exp $(-t/2T_1)$ to the time-correlation function before performing Fourier transformations in eqs 2 and 3, where T_1 represents the excited-state lifetime of a given mode and is treated as an adjustable parameter. In Figure 2a, the original $\boldsymbol{\mu}-\boldsymbol{\mu}$ correlation function without lifetime-broadening factor is plotted. In addition to a slowly decaying component reflecting rotational relaxation of the pinene, there are highly oscillating features, as

dx.doi.org/10.1021/ct200660s |J. Chem. Theory Comput. 2011, 7, 4097–4103

can be seen in the first 300 fs period of the correlation function (see the inset of Figure 2a). These oscillating components contain information about mid- and near-IR-active mode frequencies. In Figure 2b, the $\boldsymbol{\mu}-\mathbf{M}$ cross-correlation function is plotted, and its short time (up to 300 fs) region is shown in the inset. Again, the seemingly irregular oscillating pattern in the cross-correlation function is essentially produced by a superposition of various cross-correlation functions associated with intramolecular vibrational dynamics dictated by intrinsically multidimensional anharmonic potential energy surface. Before the Fourier-transformed IR and VCD spectra are presented and discussed, an important convergence issue should be briefly discussed. If the trajectory is sufficiently long and the ensemble-averaged $\boldsymbol{\mu}-\mathbf{M}$ cross-correlation is statistically acceptable, it is expected that $\langle\boldsymbol{\mu}(t)\cdot\mathbf{M}(0)\rangle = -\langle\boldsymbol{\mu}(0)\cdot\mathbf{M}(t)\rangle$.[40,54] In Figure 2c, these two cross-correlation functions are plotted for the sake of comparison. The fact that the sum (blue line) of the two shown in the same figure is very small indicates that the MD trajectory is sufficiently long, and the ensemble average required to calculate the correlation function is reasonably good.

3.2. Fourier-Transformed IR Absorption and VCD Spectra. Using the $\boldsymbol{\mu}-\boldsymbol{\mu}$ and $\boldsymbol{\mu}-\mathbf{M}$ correlation functions, one can readily calculate their Fourier-transforms that correspond to IR absorption and VCD spectra, after treating the lifetime broadening in an ad hoc manner (see the caption of Figure 3 for mode-dependent lifetimes used here). In Figure 3, the fundamental transition bands in the frequency range from 800 to 3300 cm^{-1} are shown (see black lines), where the red lines are the experimentally measured spectra that can be found in ref 11. The IR peak intensities of fundamental transition modes vary from 1×10^{-5} to 4×10^{-5} D^2/cm^{-1}, whereas the corresponding VCD intensities are in the range from -2×10^{-9} to 2×10^{-9} D^2/cm^{-1}. Therefore, the ratio $\Delta A/A$ is estimated to be about 10^{-4}, which is fully consistent with the experimental results. The delocalized C−C stretching (800−1350 cm^{-1}), C−H bending (1350−1550 cm^{-1}), C═C stretching (1600−1700 cm^{-1}), and C−H stretching (2850−3150 cm^{-1}) bands are separately plotted in Figure 3a−d, respectively. Usually, a single scaling factor was used to correct all the ab initio calculated harmonic normal-mode frequencies of an isolated molecule—note that, for HF/6-31G method, the corresponding scaling factor used quite often is 0.8953.[55] However, for the sake of comparisons with experimental results, we use slightly different scaling factors for the four different groups of normal modes (see the caption of Figure 3). In the cases of the C−C stretching bands, the peak positions in the simulated IR absorption and VCD spectra cannot be directly matched to those in the experimental spectra. Nevertheless, a few strong features, such as the intense positive VCD peak at ∼1100 cm^{-1} and the negative VCD peak at 1050 cm^{-1}, are well reproduced by the QM/MM MD simulation.

The agreement between theory and experiment is excellent for the C−H bending IR and VCD bands appearing in the frequency range from 1425 to 1500 cm^{-1} (Figure 3b). The negative−positive (from low- to high-frequency region) couplet feature in the corresponding VCD spectrum is clearly visible. The IR absorption and VCD spectra of C═C stretching vibration are also in quantitative agreement with experimental results (see Figure 3c). However, the agreement between the simulated C−H stretching IR and VCD spectra and the experimental results is less quantitative in comparison to those of C−H bending and C═C stretching bands. Nonetheless, the overall VCD spectral pattern, i.e., "W"-form line shape, is nicely reproduced by the present simulation method. In summary, we find that: (1) the numerically simulated IR and VCD spectra of highly delocalized low-frequency C−C backbone stretching vibrations are still difficult to be accurately reproduced by the present QM/MM MD simulation method in combination with classical time-correlation function approach, (2) the line shapes of C−H bend and C═C stretch IR and VCD spectra are successfully simulated, and (3) the W-shape spectral feature of the C−H stretch VCD spectrum is in fair agreement with experimental result.

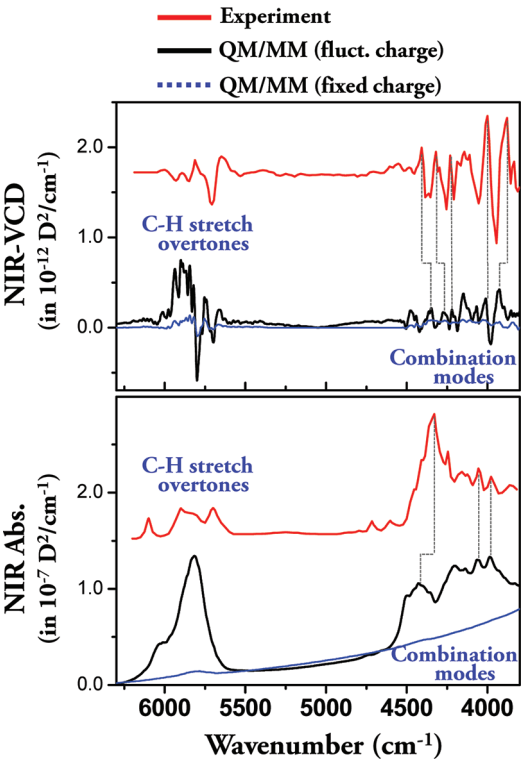

Figure 4. Numerically simulated near-IR absorption and VCD spectra. The red lines represent experimentally measured IR absorption and VCD spectra reported in ref 11. The black lines are the simulated spectra obtained by using the QM/MM MD trajectory and eq 1. The blue lines are the simulated spectra with fixed atomic partial charges. The frequency correction factor for theses C−H overtone and combination modes is 0.8953, and the lifetimes are assumed to be 300 fs. Note that the NIR absorption and NIR-VCD intensities are given in 10^{-7} and 10^{-12} D^2/cm^{-1}, respectively.

3.3. Near-IR Absorption and VCD Spectra. An important advantage of the present time-correlation function approach is that the direct Fourier transform of the corresponding correlation function provides both mid- and near-IR spectra simultaneously, as long as the time step for numerically calculated correlation function is sufficiently small. The NIR region of the vibrational spectrum contains information on resonant frequencies of a variety of overtone and combination modes. In the present case of the pinene, there are two NIR bands in the frequency range from 3800 to 6100 cm^{-1}, as can be seen in Figure 4. Again, the experimentally measured IR and VCD spectra (red lines) are given in the figure for the sake of direct comparisons. Here, the NIR absorption peak intensities of both combination and the overtone transition modes are in the range from 0.4×10^{-9} to 1.8×10^{-9} D^2/cm^{-1}, whereas the corresponding NIR-VCD peak intensities vary from -2×10^{-12} to

dx.doi.org/10.1021/ct200660s |J. Chem. Theory Comput. 2011, 7, 4097–4103

2×10^{-12} D^2/cm^{-1}. Therefore, the ratio $\Delta A/A$ in the NIR frequency region is about 10^{-4} or 10^{-5}, which is again consistent with the experimental results. Furthermore, the relative IR or VCD intensities of fundamental transitions modes are found to be 2−3 orders of magnitude larger than those of combination or overtone transition modes (compare the *y*-axis scales of Figure 4 with those of Figure 3).

In the NIR absorption spectrum, the overtone transition band of C−H stretching vibrations appears in a high-frequency region (5500−6100 cm^{-1}). Despite that the experimental spectrum exhibits three peaks, our spectrum appears to be broad and featureless except for a shoulder band in the high-frequency side. Now, the lower frequency band (3800−4700 cm^{-1}) originates from transitions of various combination modes. In ref 11 it was shown that the combination band consists of three sub-bands, i.e., combination of C−H and C−C stretch (3800−4200 cm^{-1}), combination of C−H stretch and C−H bend (4200−4500 cm^{-1}), and combination of C−H (in C═CH group) and C═C stretch (4500−4700 cm^{-1}). Despite that there exist certain discrepancies in the spectral intensity distribution between the theoretical and experimental spectra, the present time-correlation function approach utilizing HF/6-31G/MM MD trajectory correctly provides information on the peak positions of combination and the first C−H stretching overtone bands.

We next consider the numerically simulated C−H overtone and combination VCD spectra shown in the upper panel of Figure 4. Although the positive−negative alternating features in the combination band (3800−4700 cm^{-1}) are fairly well reproduced by the simulated spectrum, the overall intensity distribution and precise peak positions are not. Furthermore, the peak pattern of the C−H overtone band found in the experimentally measured VCD spectrum is not quantitatively reproduced by the simulated spectrum. Note that the VCD spectral pattern results from complicated superposition of a number of positive and negative features. Consequently, any inaccuracy in predicting frequencies of anharmonic vibrational modes would lead to significantly distorted spectrum deviating from experiment. However, even though typical IR absorption and VCD intensities of the combination and overtone bands are 1−2 orders of magnitude smaller than the fundamental transition bands, such weak features are clearly visible in the simulated NIR absorption and VCD spectra obtained from the calculated $\boldsymbol{\mu}-\boldsymbol{\mu}$ and $\boldsymbol{\mu}-\mathbf{M}$ time-correlation functions. This strongly indicates that the molecular dynamics of the pinene on the QM anharmonic potential energy surface is clearly better than that on the classical mechanical potential energy surface constructed by MM force fields.

3.4. Fluctuating Charge Effects on NIR Spectra. As can be seen in eq 1, the fluctuating electric and magnetic dipoles are determined by time-dependent atomic partial charges, coordinates and velocities. In the case of the MM MD simulation, the atomic partial charges are often assumed to be constants so that the polarizable nature of the solute molecule is completely ignored. However, in the present QM/MM MD simulation, fluctuating atomic partial charges due to solute−solvent interactions were constantly updated and saved for subsequent calculations of electric and magnetic dipole moments. Now, to investigate the precise effect of the solute polarization on vibrational spectra, we deliberately consider the average atomic partial charges, instead of time-dependent ones, when the electric and magnetic dipole moments are calculated, i.e., $\boldsymbol{\mu}(t) \cong \Sigma_i \langle q_i \rangle \mathbf{r}_i(t)$ and $\mathbf{M}(t) \cong (1/2c)\Sigma_i \langle q_i \rangle \mathbf{r}_i(t) \times \mathbf{v}_i(t)$, where $\langle q_i \rangle$ represents the average partial charge of the *i*th atom. In Table 1, the atomic partial charges averaged over the 1 ns QM/MM MD trajectory as well as their standard deviations are given. The standard deviations of fluctuating atomic partial charges are fairly small, which is because the solute molecule, pinene, is relatively rigid and the surrounding nonpolar solvent molecules CCl_4 weakly perturb the electronic structure of the pinene.

Table 1. Average Atomic Partial Charges and Their Standard Deviations in Parentheses of (1*S*)-(−)-*β*-Pinene Obtained From QM/MM MD Simulation Trajectory[a]

atom type	atomic partial charge (in unit *e*)
C1	−0.017 (0.014)
C2	−0.210 (0.010)
C3	−0.281 (0.011)
C4	−0.373 (0.017)
C5	0.165 (0.019)
C6	−0.295 (0.016)
C7	−0.424 (0.016)
C8	−0.272 (0.011)
C9	−0.435 (0.013)
C10	−0.446 (0.016)
H11 (-C2)	0.160 (0.008)
H12 (-C3)	0.161 (0.008)
H13 (-C3)	0.164 (0.008)
H14 (-C4)	0.183 (0.009)
H15 (-C4)	0.177 (0.009)
H16 (-C6)	0.165 (0.009)
H17 (-C7)	0.154 (0.011)
H18 (-C7)	0.157 (0.011)
H19 (-C8)	0.161 (0.008)
H20 (-C8)	0.171 (0.008)
H21 (-C9)	0.156 (0.009)
H22 (-C9)	0.154 (0.009)
H23 (-C9)	0.155 (0.009)
H24 (-C10)	0.155 (0.011)
H25 (-C10)	0.156 (0.011)
H26 (-C10)	0.157 (0.011)

[a] Atom types are displayed in Figure 1.

Using the approximate $\boldsymbol{\mu}(t)$ and $\mathbf{M}(t)$ with fixed atomic partial charges, we calculated the corresponding time-correlation functions and obtained the simulated IR absorption and VCD spectra (see the blue lines in Figures 3 and 4). The simulated C−C stretch, C−H bend, C═C stretch spectra with fixed charges are quantitatively similar to those with fluctuating charges. In contrast, the high-frequency C−H stretch, overtone, and combination spectra, as can be seen in Figures 3d and 4, are strongly dependent on whether the polarizable nature of the solute is taken into consideration or not. Particularly, if the solute is treated as a nonpolarizable molecule, the NIR absorption and VCD band intensities are negligibly smaller than those with fluctuating atomic partial charges. This is an interesting observation because it suggests that the polarizable nature of a given solute is quite important in the determination of the dipole and rotational strengths of high-frequency modes. On the other hand, the transition dipole and the rotational strengths of low-frequency modes are largely determined by structural fluctuation

amplitudes, i.e., standard deviations of fluctuating atomic coordinates and velocities. This can be understood by noting that the low-frequency modes are typically large-amplitude vibrations in comparison to those of high-frequency vibrations—note that the root-mean-square of vibrational displacement is inversely proportional to $(\mu\omega)^{1/2}$, where μ and ω are the reduced mass and angular frequency, respectively. Thus, the present computational studies clearly show that the polarizable nature of molecular vibrations is absolutely necessary to quantitatively describe NIR absorption and VCD phenomena of chiral molecules in condensed phases.

4. SUMMARY

In the present paper, we showed that the time-correlation function approaches with QM/MM MD simulation methods are useful to simulate not only mid-IR but also near-IR absorption and VCD spectra of chiral molecules in solutions. Not only the complicated solute−solvent interaction-induced effects on vibrational line shapes but also the polarization effects on dipole and rotational strengths were fully taken into account by employing QM treatment of the solute and MM description of interacting solvent molecules. Since the molecular vibrational dynamics is fully determined by quantum mechanically calculated potential energy surface with approximate QM/MM solute−solvent interactions, not only the fundamental but also the overtone and combination mode transitions were correctly included without relying on local mode approximations. However, due to the limited accuracies of classical expressions for the electric and magnetic dipole moments with approximate QM/MM solute−solvent interactions, the mid- and near-IR absorption and VCD spectra of low-frequency C−C stretching and C−H overtone modes were found to deviate from experimental results. We believe that such a lack of chemical accuracy in simulating NIR spectra can be overcome by employing a better QM method and by performing sufficiently long MD simulations. Nevertheless, we anticipate that the general strategy utilizing time-correlation function theory in combination with ab initio QM/MM MD simulation method will be of critical use in quantitatively simulating a variety of vibrational spectra including near-IR VCD.

AUTHOR INFORMATION

Corresponding Author

*E-mail: mcho@korea.ac.kr.

Notes

The authors declare no competing financial interest.

ACKNOWLEDGMENT

This work was supported by the National Research Foundation of Korea (NRF) grants funded by the Korea government (MEST) (nos. 20090078897 and 20110020033) and by the financial support from the Korea Basic Science Institute (T31401) grant to M.C. Also, we thank an anonymous reviewer for suggesting us to replot Figures 3 and 4 with proper intensity scales.

REFERENCES

(1) In *Near-Infrared Spectroscopy: Principles, Instruments, Applications*; Siesler, H. W., Ozaki, Y., Kawata, S., Heise, H. M., Eds.; Wiley-VCH: Weinheim, Germany, 2002.
(2) Sage, M. L.; Jortner, J. *Adv. Chem. Phys.* **1981**, *47*, 293–322.
(3) Child, M. S.; Halonen, L. *Adv. Chem. Phys.* **1985**, *57*, 1–58.
(4) Donaldson, D. J.; Tuck, A. F.; Vaida, V. *Chem. Rev.* **2003**, *103*, 4717–4730.
(5) Wolf, M.; Ferrari, M.; Quaresima, V. *J. Biomed. Opt.* **2007**, *12*, 062104.
(6) Jobsis, F. F. *Science* **1977**, *198*, 1264–1267.
(7) Chýlek, P.; Geldart, D. J. W. *Geophys. Res. Lett.* **1997**, *24*, 2015–2018.
(8) Child, M. S. *Acc. Chem. Res.* **1985**, *18*, 45–50.
(9) Henry, B. R. *Acc. Chem. Res.* **1987**, *20*, 429–435.
(10) Abbate, S.; Castiglioni, E.; Gangemi, F.; Gangemi, R.; Longhi, G. *Chirality* **2009**, *21*, E242–E252.
(11) Guo, C.; Shah, R. D.; Dukor, R. K.; Freedman, T. B.; Cao, X.; Nafie, L. A. *Vib. Spectrosc.* **2006**, *42*, 254–272.
(12) Hsu, E. C.; Holzwarth, G. *J. Chem. Phys.* **1973**, *59*, 4678–4685.
(13) Nafie, L. A.; Dukor, R. K.; Roy, J.-R.; Rilling, A.; Cao, X.; Buijs, H. *Appl. Spectrosc.* **2003**, *57*, 1245–1249.
(14) Cao, X.; Shah, R. D.; Dukor, R. K.; Guo, C.; Freedman, T. B.; Nafie, L. A. *Appl. Spectrosc.* **2004**, *58*, 1057–1064.
(15) Guo, C.; Shah, R. D.; Mills, J.; Dukor, R. K.; Cao, X.; Freedman, T. B.; Nafie, L. A. *Chirality* **2006**, *18*, 775–782.
(16) Keiderling, T. A.; Stephens, P. J. *Chem. Phys. Lett.* **1976**, *41*, 46–48.
(17) Abbate, S.; Longhi, G.; Givens, J. W.; Boiadjiev, S. E.; Lightner, D. A.; Moscowitz, A. *Appl. Spectrosc.* **1996**, *50*, 642–643.
(18) Abbate, S.; Longhi, G.; Boiadjiev, S.; Lightner, D. A.; Bertucci, C.; Salvadori, P. *Enantiomer* **1998**, *3*, 337–347.
(19) Castiglioni, E.; Lebon, F.; Longhi, G.; Abbate, S. *Enantiomer* **2002**, *7*, 161–173.
(20) Abbate, S.; Longhi, G.; Santina, C. *Chirality* **2000**, *12*, 180–190.
(21) Abbate, S.; Castiglioni, E.; Gangemi, F.; Gangemi, R.; Longhi, G.; Ruzziconi, R.; Spizzichino, S. *J. Phys. Chem. A* **2007**, *111*, 7031–7040.
(22) Longhi, G.; Gangemi, R.; Lebon, F.; Castiglioni, E.; Abbate, S.; Pultz, V. M.; Lightner, D. A. *J. Phys. Chem. A* **2004**, *108*, 5338–5352.
(23) Abbate, S.; Longhi, G.; Ricard, L.; Bertucci, C.; Rosini, C.; Salvadori, P.; Moscowitz, A. *J. Am. Chem. Soc.* **1989**, *111*, 836–840.
(24) Bak, K. L.; Bludský, O.; Jørgensen, P. *J. Chem. Phys.* **1995**, *103*, 10548–10555.
(25) Polavarapu, P. L. *Mol. Phys.* **1996**, *89*, 1503–1510.
(26) Abbate, S.; Gangemi, R.; Longhi, G. *J. Chem. Phys.* **2002**, *117*, 7575–7586.
(27) Gangemi, R.; Longhi, G.; Abbate, S. *Chirality* **2005**, *17*, 530–539.
(28) Gangemi, F.; Gangemi, R.; Longhi, G.; Abbate, S. *Phys. Chem. Chem. Phys.* **2009**, *11*, 2683–2689.
(29) Cheng, Y.-L.; Chen, H.-Y.; Takahashi, K. *J. Phys. Chem. A* **2011**, *115*, 5641–5653.
(30) Lehmann, K. K. *J. Chem. Phys.* **1983**, *79*, 1098–1098.
(31) Mills, I. M.; Robiette, A. G. *Mol. Phys.* **1985**, *56*, 743–765.
(32) Ricard-Lespade, L.; Longhi, G.; Abbate, S. *Chem. Phys.* **1990**, *142*, 245–259.
(33) Gangemi, F.; Gangemi, R.; Longhi, G.; Abbate, S. *Vib. Spectrosc.* **2009**, *50*, 257–267.
(34) Marcott, C.; Faulkner, T. R.; Moscowitz, A.; Overend, J. *J. Am. Chem. Soc.* **1977**, *99*, 8169–8175.
(35) Faulkner, T. R.; Marcott, C.; Moscowitz, A.; Overend, J. *J. Am. Chem. Soc.* **1977**, *99*, 8160–8168.
(36) Gorbunov, R. D.; Nguyen, P. H.; Kobus, M.; Stock, G. *J. Chem. Phys.* **2007**, *126*, 054509.
(37) Hornícek, J.; Kaprálová, P.; P., B. *J. Chem. Phys.* **2007**, *127*, 084502.
(38) Kinnaman, C. S.; Cremeens, M. E.; Romesberg, F. E.; Corcelli, S. A. *J. Am. Chem. Soc.* **2006**, *128*, 13334–13335.

(39) Schmidt, J. R.; Corcelli, S. A.; Skinner, J. L. *J. Chem. Phys.* **2004**, *121*, 8887–8896.
(40) Yang, S.; Cho, M. *J. Chem. Phys.* **2009**, *131*, 135102.
(41) Yang, S.; Cho, M. *J. Chem. Phys.* **2005**, *123*, 134503.
(42) Choi, J.-H.; Hahn, S.; Cho, M. *Biopolymers* **2006**, *83*, 519–536.
(43) Choi, J.-H.; Hahn, S.; Cho, M. *Int. J. Quantum Chem.* **2005**, *104*, 616–634.
(44) Choi, J.-H.; Lee, H.; Lee, K.-K.; Hahn, S.; Cho, M. *J. Chem. Phys.* **2007**, *126*, 045102.
(45) Jeon, J.; Yang, S.; Choi, J.-H.; Cho, M. *Acc. Chem. Res.* **2009**, *42*, 1280–1289.
(46) Bour, P.; Keiderling, T. A. *J. Phys. Chem. B* **2005**, *109*, 23687–23697.
(47) Rhee, H.; June, Y.-G.; Lee, J.-S.; Lee, K.-K.; Ha, J.-H.; Kim, Z. H.; Jeon, S.-J.; Cho, M. *Nature* **2009**, *458*, 310–313.
(48) Choi, J.-H.; Cheon, S.; Cho, M. *J. Chem. Phys.* **2010**, *132*, 074506.
(49) Rhee, H.; Choi, J.-H.; Cho, M. *Acc. Chem. Res.* **2010**, *43*, 1527–1536.
(50) Ringer, A. L.; MacKerell, A. D. *J. Phys. Chem. Lett.* **2011**, *2*, 553–556.
(51) Brooks, B. R.; Bruccoleri, R. E.; Olafson, B. D.; States, D. J.; Swaminathan, S.; Karplus, M. *J. Comput. Chem.* **1983**, *4*, 187–217.
(52) Guest, M. F.; Bush, I. J.; Van Dam, H. J. J.; Sherwood, P.; Thomas, J. M. H.; Van Lenthe, J. H.; Havenith, R. W. A.; Kendrick, J. *Mol. Phys.* **2005**, *103*, 719–747.
(53) Mulliken, R. S. *J. Chem. Phys.* **1955**, *23*, 1833–1840.
(54) Abbate, S.; Longhi, G.; Kwon, K.; Moscowitz, A. *J. Chem. Phys.* **1998**, *108*, 50–62.
(55) Scott, A. P.; Radom, L. *J. Phys. Chem.* **1996**, *100*, 16502–16513.